

See discussions, stats, and author profiles for this publication at: <https://www.researchgate.net/publication/23952463>

# Activation and cleavage of the N–O bond in dinuclear mixed-metal nitrosyl systems and comparative analysis of carbon monoxide, dinitrogen, and nitric oxide activation

ARTICLE *in* DALTON TRANSACTIONS · MARCH 2009

Impact Factor: 4.2 · DOI: 10.1039/b812568f · Source: PubMed

CITATIONS

12

READS

31

## 4 AUTHORS, INCLUDING:



[Germán E Cavigliasso](#)

Australian National University

52 PUBLICATIONS 776 CITATIONS

[SEE PROFILE](#)



[Gemma Joy Christian](#)

Avondale College of Higher Education

22 PUBLICATIONS 341 CITATIONS

[SEE PROFILE](#)



[Robert Stranger](#)

Australian National University

175 PUBLICATIONS 2,493 CITATIONS

[SEE PROFILE](#)

# Activation and cleavage of the N–O bond in dinuclear mixed-metal nitrosyl systems and comparative analysis of carbon monoxide, dinitrogen, and nitric oxide activation†

Germán Cavigliasso,<sup>a</sup> Gemma Christian,<sup>a</sup> Robert Stranger<sup>\*a</sup> and Brian F Yates<sup>b</sup>

Received 22nd July 2008, Accepted 14th October 2008

First published as an Advance Article on the web 17th December 2008

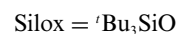
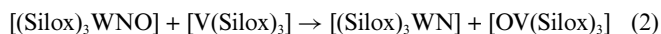
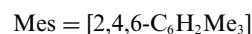
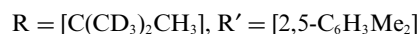
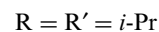
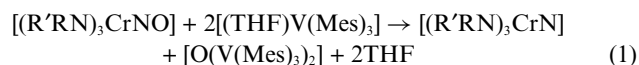
DOI: 10.1039/b812568f

The activation and scission of the N–O bond in nitric oxide using dinuclear mixed-metal species, comprising transition elements with d<sup>3</sup> and d<sup>2</sup> configurations and trisamide ligand systems, have been investigated by means of density functional calculations. The [Cr(III)–V(III)] system is analyzed in detail and, for comparative purposes, the [Mo(III)–Nb(III)], [W(III)–Ta(III)], and (mixed-row) [Mo(III)–V(III)] systems are also considered. The overall reaction and individual intermediate steps are favourable for all systems, including the case where first row (Cr and V) metals are exclusively involved, a result that has not been observed for the related dinitrogen and carbon monoxide systems. In contrast to the cleavage of dinitrogen by three-coordinate Mo amide complexes where the dinuclear intermediate possesses a linear [Mo–NN–Mo] core, the [M–NO–M'] core must undergo significant bending in order to stabilize the dinuclear species sufficiently for the reaction to proceed beyond the formation of the nitrosyl encounter complex. A comparative bonding analysis of nitric oxide, dinitrogen and carbon monoxide activation is also presented. The overall results indicate that the  $\pi$  interactions are the dominant factor in the bonding across the [M–L<sup>1</sup>L<sup>2</sup>–M'] (L<sup>1</sup>L<sup>2</sup> = N–O, N–N, C–O) moiety and, consequently, the activation of the L<sup>1</sup>–L<sup>2</sup> bond. These trends arise from the fact that the energy gaps between the  $\pi$  orbitals on the metal and small molecule fragments are much more favourable than for the corresponding  $\sigma$  orbitals. The  $\pi$  energy gaps decrease in the order [NO < N<sub>2</sub> < CO] and consequently, for each individual  $\pi$  orbital interaction, the back donation between the metal and small molecule increases in the order [CO < N<sub>2</sub> < NO]. These results are in accord with previous findings suggesting that optimization of the  $\pi$  interactions plays a central role in increasing the ability of these transition metal systems to activate and cleave small molecule bonds.

## 1 Introduction

Although nitric oxide is among the simplest of molecules, and its properties and applications have been studied extensively, research into the fundamental aspects of its chemistry remains highly significant, for example due to the biological and medicinal implications of the key role played by this molecule as a physiological regulator and metabolic intermediate.<sup>1</sup> Natural biomedical activities include its function in blood pressure control, neurotransmission, immune response and disease states. The fact that the principal targets under physiological conditions are metal sites enhances the significance of investigating the fundamental chemistry of nitric oxide in relation to its reactions and interactions with metal centres.<sup>2</sup>

Of particular relevance to understanding the varied chemistry of nitric oxide, including its biochemical and environmental roles, is the study of the activation and cleavage of the N–O bond in inorganic and organometallic nitrosyl species.<sup>3</sup> Experimental examples of the cleavage of the N–O bond in (inorganic) nitrosyl complexes are provided by the following deoxygenation reactions,<sup>4,5</sup>



Analogous reactions to that shown in eqn (2) have also been reported for related Nb(Silox)<sub>3</sub> and Ta(Silox)<sub>3</sub> complexes (used as oxygen atom acceptors).<sup>5</sup>

<sup>a</sup>Department of Chemistry, Faculty of Science, Australian National University, Canberra, ACT 0200, Australia

<sup>b</sup>School of Chemistry, University of Tasmania, Private Bag 75, Hobart, TAS 7001, Australia

† Electronic supplementary information (ESI) available: Two figures showing the different initial geometric configurations used in the optimization of the molecular structures of the encounter complexes and dinuclear intermediate species and two tables containing bonding energy and free energy results for all steps comprising the cleavage reaction profile. See DOI: 10.1039/b812568f

A remarkable find, in connection with the activation and scission of small molecules, is represented by the recent discovery<sup>6–8</sup> that three-coordinate metal complexes, such as  $[\text{Mo}(\text{N}^i\text{BuAr})_3]$ , can cleave the N–N bond in the dinitrogen molecule under mild conditions, in contrast to the rather severe temperature and pressure conditions characteristic of the corresponding industrial method, the Haber-Bosch process.<sup>9</sup> Furthermore, these complexes are extremely versatile; capable of selectively cleaving the N–N bond in  $\text{N}_2\text{O}$ ,<sup>10</sup> and also binding and activating a variety of other small molecules,<sup>11–14</sup> including CO and  $\text{CN}^-$ . In the latter two cases, however, cleavage has not been experimentally observed.

The thermodynamic driving force for the cleavage of a multiply-bonded small molecule, generically described as  $[\text{L}^1\equiv\text{L}^2]$ , is associated with the formation of strong M–L bonds in the products. Therefore, choosing metals that lead to the greatest stabilization of the products is a reasonable approach to identifying and designing systems capable of cleaving small molecules. We have recently conducted a systematic computational study of trends in M–L bond strength,<sup>15</sup> involving a range of transition metals, oxidation states, and  $d^n$  configurations, which has shown that the strongest M–C, M–N, and M–O bonds are obtained, respectively, for  $d^4$ ,  $d^3$ , and  $d^2$  metal-based electronic configurations, and that M–L bond strength is greater for the heavier members within a group, and the earlier members within a period. Additional investigations have shown that M–S bond strengths are also optimized when the metal atoms possess a  $d^2$  configuration, analogously to the case of M–O bond strengths.<sup>16</sup>

An example of the application of these principles and findings is represented by our recent computational investigations that have shown that a mixed-metal  $[d^4d^2]$  dinuclear system involving  $\text{Re}(\text{III})$  and  $\text{Ta}(\text{III})$  complexes bound to the C and O or S atoms, respectively, appears to be an excellent candidate for cleaving the C–O bond in carbon monoxide,<sup>17</sup> and the C–S bonds in both carbon sulfide and disulfide.<sup>16</sup> Moreover, for the related case of the activation and cleavage of the C–N bond in the cyanide ion, although scission has not been predicted, the most favourable conditions have been observed when a mixed-metal  $[d^4d^3]$  system, involving  $\text{Re}(\text{III})$ –C and N– $\text{W}(\text{III})$  binding, is utilized.<sup>18</sup>

Cundari and co-workers have conducted a detailed computational study of the deoxygenation reactions of the W nitrosyl species in eqn (2) for the cases where complexes of all three members of group 5 (V, Nb, Ta) are used as oxygen atom acceptors, but N–O bond cleavage by a system containing exclusively first row transition metal centres was not considered.<sup>5</sup>

The strength of the N–O bond ( $\sim 607 \text{ kJ mol}^{-1}$ ) in nitric oxide is significantly smaller than that of the N–N bond ( $\sim 942 \text{ kJ mol}^{-1}$ ) in dinitrogen and the C–O bond ( $\sim 1072 \text{ kJ mol}^{-1}$ ) in carbon monoxide. Therefore, nitric oxide cleavage using dinuclear trisamide-type complexes could be achieved, in principle, by systems involving first row (3d) transition elements, without having to resort to employing 4d or 5d metals, as is the case for dinitrogen and carbon monoxide. In this work, we explore this possibility by investigating nitric oxide activation and cleavage by a  $[\text{Cr}(\text{III})\text{--V}(\text{III})]$  system and, for comparative purposes, we also consider  $[\text{Mo}(\text{III})\text{--Nb}(\text{III})]$ ,  $[\text{W}(\text{III})\text{--Ta}(\text{III})]$ , and (mixed-row)  $[\text{Mo}(\text{III})\text{--V}(\text{III})]$  systems. All of these combinations possess the  $[d^3d^3]$  metal-based electronic configuration predicted to be most favourable for the stabilization of M–N and M–O bonds.<sup>15</sup> In addition, we present a comparative bonding analysis, performed using energy

decomposition methods, of carbon monoxide, dinitrogen, and nitric oxide activation in order to probe the relative importance of various bonding mechanisms, including metal back donation.

## 2 Computational details

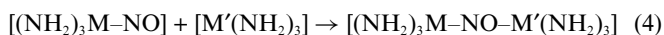
All density-functional calculations were carried out using the Amsterdam density functional (ADF 2007) package.<sup>19–21</sup> A generalized gradient approximation (GGA) functional consisting of the exchange and correlation expressions proposed by Becke<sup>22</sup> and Perdew,<sup>23</sup> respectively, was utilized. Basis sets of the all-electron type and triple-zeta quality, involving one polarization function (TZP), were employed.<sup>19–21</sup> Relativistic effects were included by means of the zero order regular approximation (ZORA).<sup>24–26</sup>

Calculations were performed in a spin-unrestricted manner, and default convergence parameters ( $10^{-3}$  Hartrees for energy and  $10^{-2}$  Hartrees/Angstrom for gradient) were used for self-consistent-field (SCF) procedures and geometry optimizations, with the integration accuracy parameter (accint) set to 4.0. Frequency calculations were carried out using analytical second derivatives,<sup>27–29</sup> with an integration accuracy of 6.0 and a gradient tolerance parameter of  $10^{-4}$  Hartrees/Angstrom for the geometry optimization step preceding the analytical approach. Plots of the molecular orbitals were generated with the MOLEKEL program<sup>30,31</sup> using data in MOLDEN format<sup>32,33</sup> derived from the ADF TAPE21 files.

The general methodology (including density functionals and basis sets) chosen for this study is analogous to that employed in our previous investigations of small molecule activation and cleavage by transition metal complexes, where it has been shown to provide a satisfactory description and treatment of a range of systems and problems.<sup>15,17,18,34–38</sup> A recent study by Swart and co-workers has also shown that the methodology inherent to the Amsterdam density functional package provides reliable and consistent results for both spin-state energy and geometry calculations.<sup>39</sup>

## 3 Results and discussion

Calculations exploring the activation and cleavage of the N–O bond in nitric oxide have been carried out using an approach equivalent to that employed in our previous computational studies involving dinitrogen,<sup>34</sup> carbon monoxide<sup>17</sup> and cyanide.<sup>18</sup> In this approach, a model system, in which  $[\text{NH}_2]$  ligands replace the bulky  $[\text{N}(\text{R})\text{Ar}]$  groups of the experimental systems, is utilized and the overall reaction process is represented as:



The structures of the reactants and products have been previously reported,<sup>15</sup> and in the present work these results have been used as initial structures for subsequent geometry optimizations. The structures of the encounter complexes and dinuclear species have been explored in detail through the testing of several possible and plausible geometric configurations, which are given as ESI.†

### 3.1 N–O bond cleavage: Cr–V system

The results for the  $[\text{Cr(III)}-\text{V(III)}]$  system are summarized in Fig. 1–3. The reaction profile in Fig. 1 shows relative energy values (with zero point corrections excluded) for the species on the lowest energy path (represented using dash lines) and also includes, for some steps, structures or spin states that lie to higher energy. The overall process is predicted to be highly exothermic, with the products stabilized by  $\sim 525 \text{ kJ mol}^{-1}$  (including zero point corrections) relative to the reactants, and both intermediate steps are also energetically favourable. Nitric oxide cleavage in the  $[\text{Cr(III)}-\text{NO}-\text{V(III)}]$  system is, thus,  $\sim 190 \text{ kJ mol}^{-1}$  and  $\sim 58 \text{ kJ mol}^{-1}$  more exothermic, respectively, than the previously reported dinitrogen  $[\text{Mo(III)}-\text{NN}-\text{Mo(III)}]$  and carbon monoxide  $[\text{Re(III)}-\text{CO}-\text{Ta(III)}]$  cleavage reactions.<sup>17,34</sup>

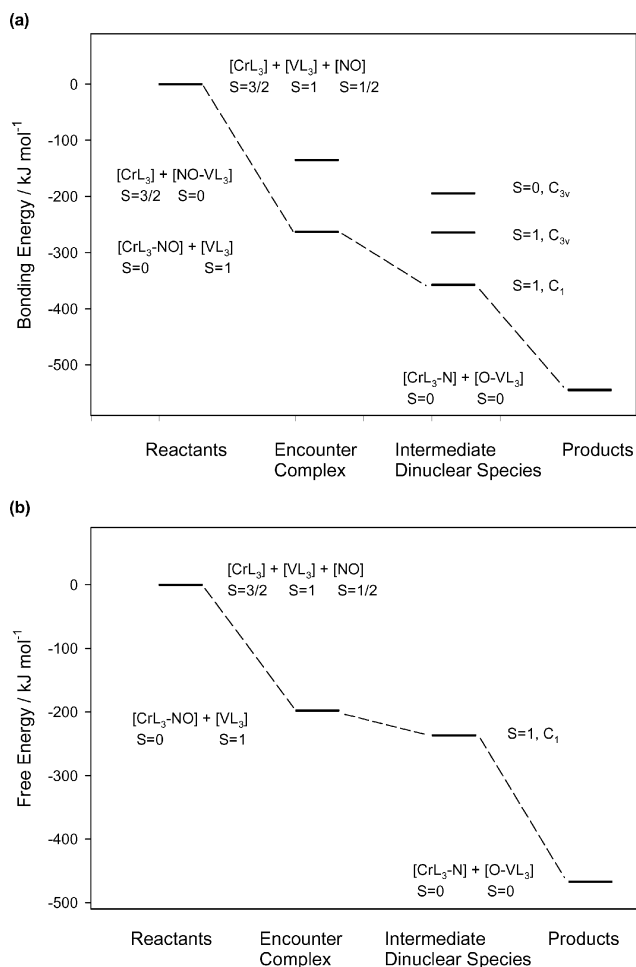


**Fig. 1** Energy profile for the overall reaction process involving  $[\text{Cr}(\text{NH}_2)_3]$ ,  $[\text{NO}]$  and  $[\text{V}(\text{NH}_2)_3]$ . All bonding energy (a) and free energy (b) values are given relative to the reactants.

The  $[\text{Cr}(\text{NH}_2)_3]$  complex in the quartet spin state binds nitric oxide more favourably (by  $\sim 128 \text{ kJ mol}^{-1}$ ) than the  $[\text{V}(\text{NH}_2)_3]$  complex in the triplet spin state and, therefore, the energetically preferred path to the formation of the intermediate dinuclear species is the binding of  $[\text{V}(\text{NH}_2)_3]$  to singlet  $[(\text{NH}_2)_3\text{Cr}-\text{NO}]$ . The predicted lowest-energy minimum configuration of the dinuclear  $[(\text{NH}_2)_3\text{Cr}-\text{NO}-\text{V}(\text{NH}_2)_3]$  species has  $C_1$  symmetry and a triplet spin state. In contrast, no minimum structure has been

computationally observed for the corresponding singlet state as the singlet surface leads to spontaneous cleavage of the N–O bond. For comparison, the relative energy values of the singlet and triplet states of the dinuclear species, obtained under  $C_{3v}$  symmetry constraints, are also given in Fig. 1. In  $C_1$  symmetry, the triplet state is stabilized by  $\sim 95 \text{ kJ mol}^{-1}$  with respect to the encounter complex, but the introduction of the  $C_{3v}$  constraints leads to significant destabilization and, in this case, the dinuclear species is either similar in energy (triplet state) to, or considerably less stable (singlet state) than, the encounter complex. Furthermore, the  $C_{3v}$  structures are not true minima.

The dissociation of the N–O bond in the dinuclear species, leading to the formation of the nitride,  $[(\text{NH}_2)_3\text{CrN}]$ , and oxide,  $[(\text{NH}_2)_3\text{VO}]$ , products has been explored by means of potential energy scans, and the results for  $C_{3v}$  and  $C_1$  symmetry are presented in Fig. 2. The potential energy curves are qualitatively similar in that, at distances close to the equilibrium N–O bond length, the triplet state is favoured, but a crossover from the triplet to singlet surface is required to yield the nitride and oxide products in their preferred singlet states. However, the minimum in the triplet curve and the crossover point occur at somewhat shorter N–O distances

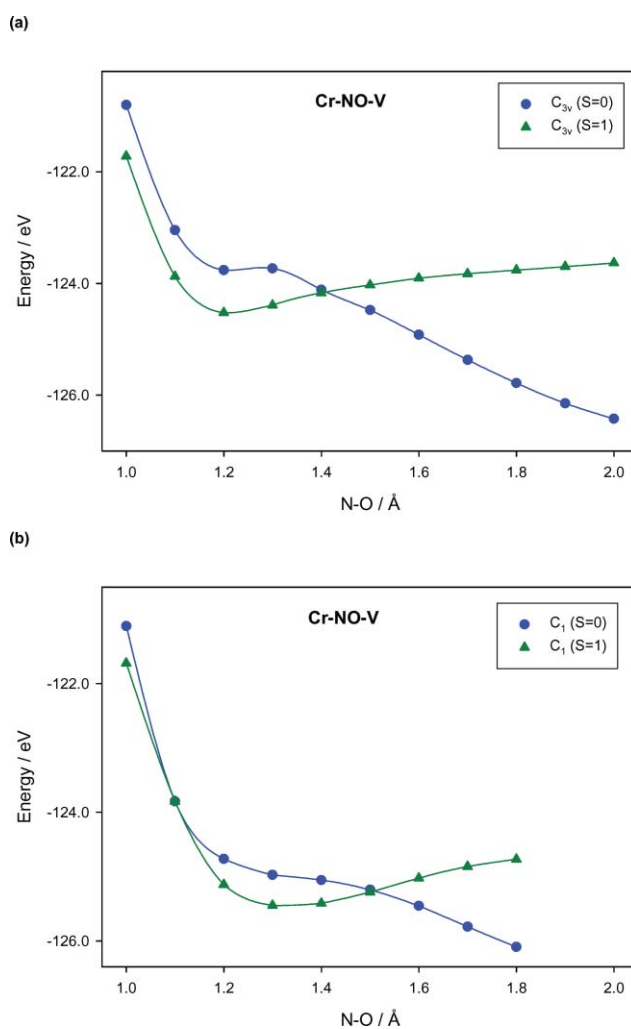


**Fig. 2** Comparison of potential energy curves obtained using (a)  $C_{3v}$  and (b)  $C_1$  symmetry, for the N–O bond dissociation of  $[(\text{NH}_2)_3\text{Cr}-\text{NO}-\text{V}(\text{NH}_2)_3]$ .

in  $C_{3v}$  relative to  $C_1$  symmetry, and the crossover barrier is rather larger in the former ( $\sim 37$  kJ mol $^{-1}$ ) than the latter ( $\sim 22$  kJ mol $^{-1}$ ). Also, whilst in  $C_{3v}$  symmetry, both the singlet and triplet curves exhibit a (small) barrier to cleavage, this phenomenon is only observed in  $C_1$  symmetry for the triplet surface, since no barrier is predicted on the singlet surface.

Relative free energy values (obtained at 298.15 K and 1.00 atm) for the species along the lowest energy path are also shown in Fig. 1. Although consideration of entropic effects reduces, to some extent, the stability (relative to reactants) of the encounter complex, dinuclear species, and products, a comparison of the two graphs in Fig. 1 indicates that enthalpic effects are the dominant factor, and the qualitative features of the overall reaction profile are similar.

Optimized structures, in the most favoured geometric configuration and spin state, for all species in the reaction profile of Fig. 1, are given in Fig. 3. It is interesting to note that some activation of the N–O bond is observed in the encounter complex, where the N–O distance is 122.2 pm compared to 116.6 pm for the unbound nitric oxide molecule. Also, the dinuclear species has a more activated N–O bond in the  $C_1$  ( $\sim 134$  pm) than  $C_{3v}$  ( $\sim 123$  pm) form, with a significant distortion from linearity of the

[Cr–NO–V] moiety, as reflected by the Cr–N–O and N–O–V angles of  $\sim 143^\circ$  and  $\sim 124^\circ$ , respectively.

### 3.2 N–O bond cleavage: Mo–Nb, W–Ta and Mo–V systems

Energy profiles for the overall reaction process are shown in Fig. 4 for the [Mo(III)–Nb(III)] and [W(III)–Ta(III)] systems, and in Fig. 5 for the (mixed-row) [Mo(III)–V(III)] system. The general qualitative features are similar to those observed in the reaction profile for the [Cr(III)–V(III)] system.

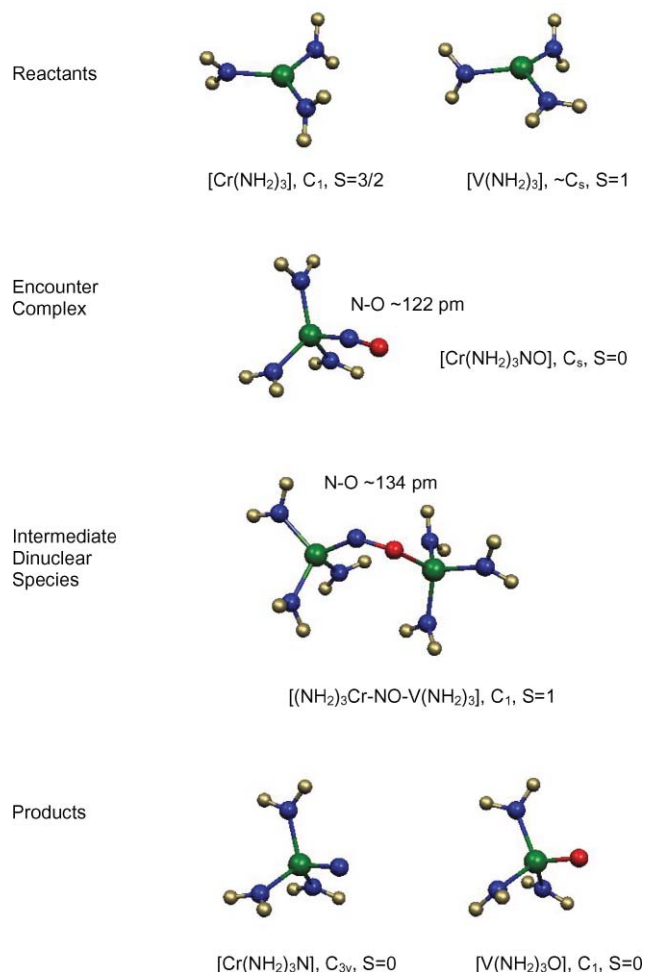


**Fig. 3** Optimized (ground-state) structures of reactants, encounter complex, intermediate dinuclear species, and products in the overall reaction process involving [Cr(NH<sub>2</sub>)<sub>3</sub>], [NO] and [V(NH<sub>2</sub>)<sub>3</sub>].

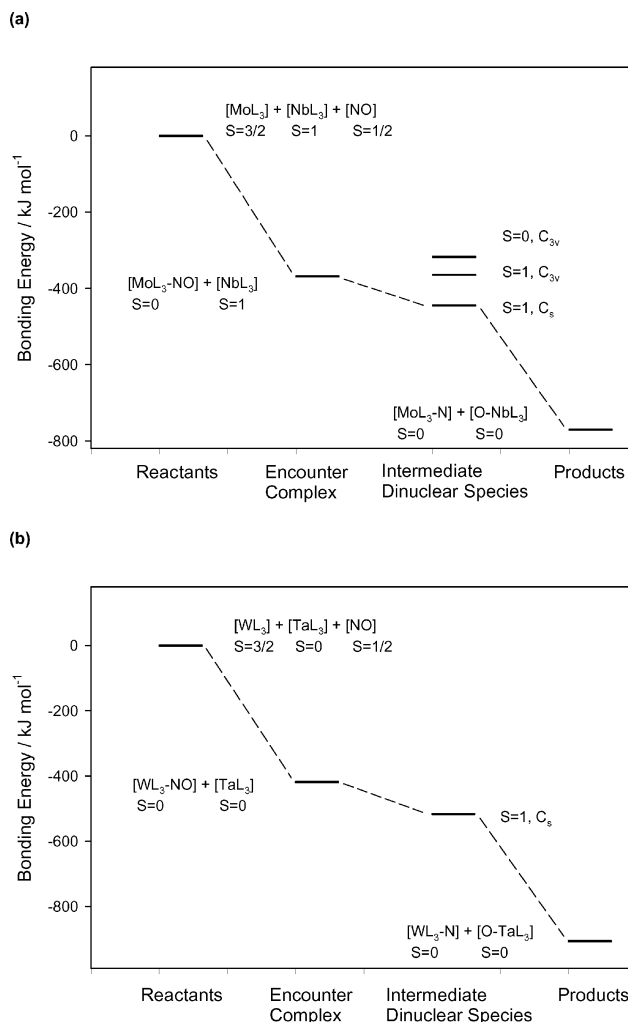


**Fig. 4** Energy profile for the overall reaction process involving (a) [Mo(NH<sub>2</sub>)<sub>3</sub>], [NO] and [Nb(NH<sub>2</sub>)<sub>3</sub>]. (b) [W(NH<sub>2</sub>)<sub>3</sub>], [NO] and [Ta(NH<sub>2</sub>)<sub>3</sub>]. All energy values are given relative to the reactants.

In all cases, the overall process is highly exothermic, with the predicted stabilization of products with respect to reactants being  $\sim 771$  kJ mol $^{-1}$ ,  $\sim 906$  kJ mol $^{-1}$ , and  $\sim 684$  kJ mol $^{-1}$  for the Mo–Nb, W–Ta and Mo–V systems, respectively. The general trend in reaction energetics, across the four systems studied in this work, thus correlates with the previously calculated trends in the strengths of M–N and M–O bonds, as both results indicate increasing stability as a transition metal group is descended.

The intermediate steps along the lowest-energy path, which involve a dinuclear species in a spin triplet state and a low-symmetry ( $C_s$  or  $C_1$ ) geometric configuration, are also



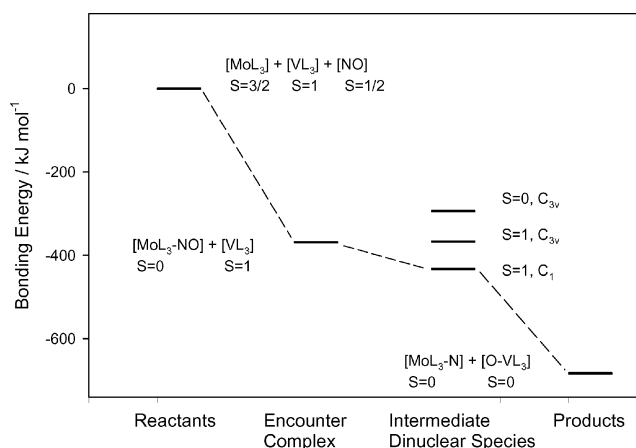


**Fig. 5** Energy profile for the overall reaction process involving  $[\text{Mo}(\text{NH}_2)_3]$ ,  $[\text{NO}]$  and  $[\text{V}(\text{NH}_2)_3]$ . All energy values are given relative to the reactants.

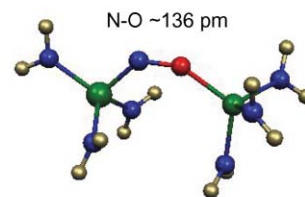
energetically favourable. If  $C_{3v}$  symmetry constraints are enforced, however, the dinuclear structures are destabilized and, in the spin triplet state, exhibit approximately the same relative energy as the encounter complex. This result applies only to the Mo–Nb and Mo–V systems, since in the W–Ta case, it has not been possible to obtain a stable dinuclear species due to the fact that, in both the singlet and triplet states, the  $[\text{W–NO–Ta}]$  structures undergo spontaneous dissociation into the metal–nitride and metal–oxide products.

In all cases involving 4d and 5d metals, the geometry optimizations of the dinuclear species were considerably more difficult to converge than for the Cr–V system, and for most of the low-symmetry configurations tested, strong distortions are observed, which render the calculated structures unrepresentative as a model for the real systems due to the presence of incorrect connectivity patterns between the fragments. The predicted lowest-energy (low-symmetry) structures, among those possessing the correct overall connectivity, are shown in Fig. 6.

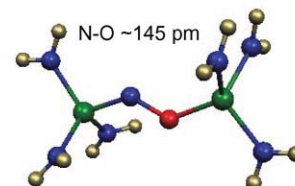
As found for the Cr–V system, the  $[\text{M–NO–M}']$  moiety exhibits significant deviations from linearity and the N–O distances suggest considerably more activation than in the  $C_{3v}$  counterparts, for which the N–O bond lengths are ~124 pm and ~123 pm in the  $[\text{Mo–NO–Nb}]$  and  $[\text{Mo–NO–V}]$  structures, respectively. A comparison of the N–O distances across the four systems investigated, in both the low-symmetry and  $C_{3v}$  cases, reveals that a similar degree of N–O activation, 123–124 pm ( $C_{3v}$ ) and 134–136 pm ( $C_s$  or  $C_1$ ), occurs when 3d and 4d metals are involved, but significantly greater activation, 145 pm ( $C_s$ ), is observed for 5d metals. The fact that a similar level of N–O activation is observed in the  $C_{3v}$  dinuclear intermediates and associated nitrosyl encounter complexes implies that the binding of the second  $[\text{M}'(\text{NH}_2)_3]$  fragment to the latter is relatively weak when the  $[\text{M–NO–M}']$  core is forced to be linear.

The calculation of potential energy scans for N–O dissociation was also considerably more difficult for the Mo–Nb, W–Ta, and Mo–V systems than in the Cr–V case. However, on a qualitative basis, the dissociation behaviour appears to be similar for all four dinuclear species. Although the singlet curve is the more favourable path to the nitride and oxide products, the triplet state of the dinuclear intermediate is more stable at distances close to the

**(a)**  $[(\text{NH}_2)_3\text{Mo–NO–Nb}(\text{NH}_2)_3]$ ,  $C_s$ ,  $S=1$



**(b)**  $[(\text{NH}_2)_3\text{W–NO–Ta}(\text{NH}_2)_3]$ ,  $C_s$ ,  $S=1$



**(c)**  $[(\text{NH}_2)_3\text{Mo–NO–V}(\text{NH}_2)_3]$ ,  $C_1$ ,  $S=1$

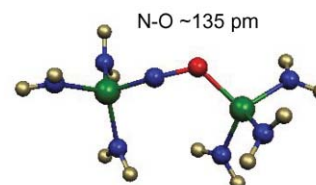


**Fig. 6** Optimized (ground-state) structures of the intermediate dinuclear species for (a) Mo–NO–Nb, (b) W–NO–Ta and (c) Mo–NO–V systems.

equilibrium N–O bond length, and therefore a crossover from the triplet to singlet surface is predicted at an N–O distance between 140–150 pm.

It is relevant to note that experimental studies of  $\text{N}_2\text{O}$  cleavage by three-coordinate Mo(III) complexes<sup>10</sup> have shown that the exclusive products are metal nitride and nitrosyl species, with no observation of N–O bond scission for the latter. The present calculations for the Cr–V, Mo–Nb, and Mo–V systems suggest that, if bending of the  $[\text{M–N–O–M}']$  core and formation of low-symmetry structures are viable, the dinuclear species should be thermodynamically stable relative to the encounter complex. However, if  $C_{3v}$  symmetry constraints are enforced, computational results incorporating enthalpic and entropic factors indicate that the dinuclear species are destabilized by ~50–60 kJ mol<sup>−1</sup> with respect to the encounter complex. A similar result has been obtained for the analogous  $[\text{Mo(III)–Mo(III)}]$  system restricted to  $C_{3v}$  symmetry, with the dinuclear intermediate destabilized by ~60 kJ mol<sup>−1</sup> relative to the encounter complex. Therefore, a possible explanation for the failure to observe cleavage of the N–O bond in the Mo nitrosyl product of the experimental system may lie in the possibility that the actual experimental structures, which contain bulky amide ligands, exhibit geometric constraints similar to those of the ( $C_{3v}$ ) model systems, rendering the reaction process unfavourable beyond the encounter complex step.

Interestingly, deoxygenation is observed, most likely *via* a dinuclear  $[\text{L}_3\text{Cr-NO-VL}'_3]$  intermediate, for the reaction in (eqn (1)). Presumably, the reduced steric bulk associated with the  $[\text{V}(\text{Mes})_3]$  centre may allow sufficient bending of the  $[\text{Cr-NO-V}]$  core so that N–O cleavage is possible. The theoretical study of the deoxygenation of  $[(\text{Silox})_3\text{WNO}]$  by  $[\text{M}(\text{Silox})_3]$  ( $\text{M} = \text{V}, \text{Nb}, \text{Ta}$ ) species described in eqn (2), also highlighted the necessity for bending of the  $[\text{W-NO-M}]$  core in order for oxygen atom transfer to occur.<sup>5</sup> The bent structure allows  $[\sigma/\pi]$  mixing to take place, thereby lowering the singlet–triplet barrier and facilitating the intersystem crossing required to form the singlet nitride and oxide products.

### 3.3 Comparative bonding analysis

In a previous publication,<sup>18</sup> we reported a bonding analysis of small molecule activation in dinuclear 5d metal complexes. This analysis was carried out by means of an energy decomposition approach, and in the present work we have used a similar procedure to conduct a comparative study of bonding interactions in the activation of nitric oxide by 3d (Cr–V) and 4d (Mo–Nb) metal systems, and dinitrogen and carbon monoxide by, respectively, 4d (Mo–Mo) and 5d (Re–Ta) metal systems.

The energy decomposition analysis<sup>40,41</sup> is performed by combining a fragment approach to the molecular structure of a chemical system with the decomposition of the total bonding energy ( $E_{\text{B}}$ ) as

$$E_{\text{B}} = E_{\text{E}} + E_{\text{P}} + E_{\text{O}} \quad (6)$$

where  $E_{\text{E}}$ ,  $E_{\text{P}}$  and  $E_{\text{O}}$ , are the electrostatic interaction, Pauli repulsion, and orbital interaction terms, respectively. A detailed description of the physical significance of these properties has been given by Bickelhaupt and Baerends.<sup>42</sup>

The bonding energy ( $E_{\text{B}}$ ) can be considered a measure of the “instantaneous” interactions between the fragments in the molecule, but does not represent the bond dissociation energy ( $E_{\text{D}}$ ), which is defined as:

$$E_{\text{D}} = E_{\text{B}} + E_{\text{F}} \quad (7)$$

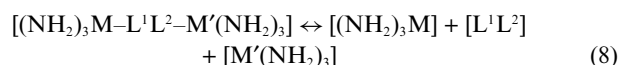
and contains, in addition to the bonding energy, a contribution ( $E_{\text{F}}$ ) arising from the fragment preparation process. This process can be described as the energy associated with the transformation of the fragments from their equilibrium geometric and electronic states into their “intrinsic” geometric and electronic states in the molecule.

The electrostatic ( $E_{\text{E}}$ ) term is calculated from the superposition of the unperturbed fragment densities at the molecular geometry, and corresponds to the classical electrostatic effects associated with Coulombic attraction and repulsion. The electrostatic contribution is generally dominated by the nucleus–electron attractions and therefore has a stabilizing influence. The Pauli ( $E_{\text{P}}$ ) term arises from the requirement that electronic anti-symmetry conditions be satisfied and is associated with repulsive four-electron two-orbital interactions. This contribution, therefore, has a destabilizing effect. The orbital interaction ( $E_{\text{O}}$ ) term represents a stabilizing factor originating from the relaxation of the molecular system due to the mixing of occupied and unoccupied orbitals, and can involve electron-pair bonding, charge-transfer or donor–acceptor interactions, and polarization.

**Table 1** Energy gaps,  $\Delta E(\sigma)$  and  $\Delta E(\pi)$ , between the relevant  $\sigma$ -like and  $\pi$ -like fragment orbitals in  $[(\text{NH}_2)_3\text{M-L}^1\text{L}^2-\text{M}'(\text{NH}_2)_3]$  systems. The  $\Delta E(\sigma)$  value corresponds to the energy difference between the unoccupied  $\text{d}_{\sigma}(\text{M})$  orbitals and the occupied  $\sigma(\text{L}^1\text{L}^2)$  orbitals, whilst the  $\Delta E(\pi)$  value is the energy difference between occupied  $\text{d}_{\pi}(\text{M})$  orbitals and the unoccupied or partially occupied  $\pi^*(\text{L}^1\text{L}^2)$  orbitals. Results correspond to calculations on  $[(\text{NH}_2)_3\text{M-L}^1\text{L}^2]$  and  $[\text{L}^1\text{L}^2-\text{M}'(\text{NH}_2)_3]$  species, with the M–L<sup>1</sup> and L<sup>2</sup>–M' distances fixed at 300 pm and the remaining structural parameters taken from the optimized  $C_{3v}$  geometry

$[(\text{NH}_2)_3\text{M-L}^1\text{L}^2-\text{M}'(\text{NH}_2)_3]$	$\Delta E(\sigma)/\text{eV}$		$\Delta E(\pi)/\text{eV}$	
	M	M'	M	M'
$[(\text{NH}_2)_3\text{Cr-NO-V}(\text{NH}_2)_3]$	6.91	7.48	0.59	0.19
$[(\text{NH}_2)_3\text{Mo-NO-Nb}(\text{NH}_2)_3]$	6.77	7.17	0.76	0.54
$[(\text{NH}_2)_3\text{Mo-NN-Mo}(\text{NH}_2)_3]$	6.27	6.27	2.17	2.17
$[(\text{NH}_2)_3\text{Re-CO-Ta}(\text{NH}_2)_3]$	4.66	5.06	2.52	1.04

The “fragmentation” scheme used for the study of the bonding interactions can be represented as:



where the small molecule  $[\text{L}^1\text{L}^2]$  fragment corresponds to N–O, N–N or C–O. In order to separate the  $\sigma$  and  $\pi$  components of the orbital interaction term, the calculations employ  $C_{3v}$  symmetry. For the four systems investigated, the dinuclear species is most stable in the triplet spin state.

It should be noted that the orbital occupation schemes chosen for the fragments attempt to reproduce, as adequately as possible, the bonding interactions in the dinuclear species. Since the electronic structure of the fragments may not necessarily correspond to the most stable electronic configuration these fragments would possess as isolated species, the trends in the energy terms and not their absolute values are of significance in the present study.

Fig. 7 contains spatial plots of the molecular orbitals that are associated with the primary  $\sigma$  (a.) and  $\pi$  (e) interactions in the dinuclear species whilst Table 1 details the corresponding energy gaps, labelled  $\Delta E(\sigma)$  and  $\Delta E(\pi)$ , respectively, between  $\sigma$ -like and  $\pi$ -like orbitals on the metal and small molecule fragments. As a consequence of the much smaller energy gaps between the metal  $\text{d}_{\pi}$  orbitals and the small molecule  $\pi^*(\text{L}^1\text{L}^2)$  orbitals compared to the corresponding separation between the metal  $\text{d}_{\sigma}$  and small molecule  $\sigma(\text{L}^1\text{L}^2)$  orbitals, the orbital plots reveal significantly greater metal character and mixing associated with the  $\pi$  compared to  $\sigma$  interactions, for all four systems.

The results of the energy decomposition analysis, based on the fragmentation scheme in eqn (8), are summarized in Tables 2 and 3. Also included in Table 2 is a structural parameter, labelled  $\Delta d$ , representing the difference in the small molecule bond distance in the dinuclear species relative to the unbound case, which can be used as a measure of the degree of small molecule activation. Selected bond distances and atomic charges, based on a Mulliken population analysis, are given in Table 4.

The Pauli and electrostatic terms are “pre-relaxation” effects in the sense that these terms are calculated before electronic relaxation of the overall system can take place through application of a self-consistent-field approach. Therefore, the magnitude of both components can be correlated with the extent of electronic overlap between the separated un-relaxed fragments. The trends observed in Table 2 are consistent with the increasing size of the

**Table 2** Energy decomposition analysis of  $[(\text{NH}_2)_3\text{M}-\text{L}^1\text{L}^2-\text{M}'(\text{NH}_2)_3]$  systems ( $E_{\text{B}}$  = total bonding energy,  $E_{\text{P}}$  = Pauli repulsion,  $E_{\text{E}}$  = electrostatic interaction,  $E_{\text{O}}$  = orbital interaction). The  $\Delta d$  parameter measures the difference in the small molecule bond distance, in the dinuclear species relative to the unbound case. Results correspond to  $C_{3v}$  symmetry

$[(\text{NH}_2)_3\text{M}-\text{L}^1\text{L}^2-\text{M}'(\text{NH}_2)_3]$	$\Delta d/\text{pm}$	$E_{\text{B}}/\text{eV}$	$E_{\text{P}}/\text{eV}$	$E_{\text{E}}/\text{eV}$	$E_{\text{O}}(\text{total})/\text{eV}$	$E_{\text{O}}(\text{a}_1)/\text{eV}$	$E_{\text{O}}(\text{e})/\text{eV}$
$[(\text{NH}_2)_3\text{Cr}-\text{NO}-\text{V}(\text{NH}_2)_3]$	5.9	-6.18	9.59	-3.74	-12.02	-2.33	-9.69
$[(\text{NH}_2)_3\text{Mo}-\text{NO}-\text{Nb}(\text{NH}_2)_3]$	7.5	-7.37	10.58	-4.14	-13.81	-2.63	-11.18
$[(\text{NH}_2)_3\text{Mo}-\text{NN}-\text{Mo}(\text{NH}_2)_3]$	9.6	-6.72	12.70	-6.47	-12.94	-3.37	-9.57
$[(\text{NH}_2)_3\text{Re}-\text{CO}-\text{Ta}(\text{NH}_2)_3]$	8.7	-7.09	13.79	-9.31	-11.58	-4.00	-7.58

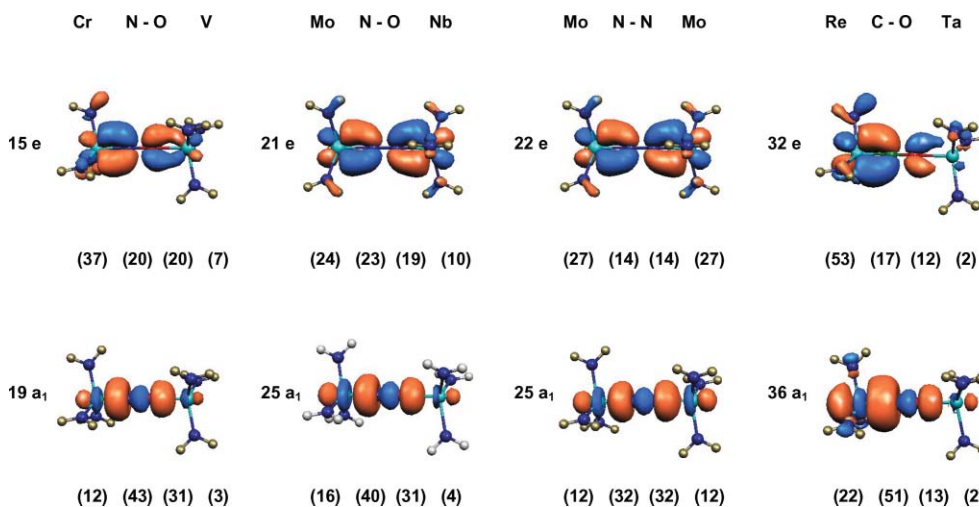


**Fig. 7** Spatial plots (in  $C_{3v}$  symmetry) for the principal orbital interactions between the metal and small molecule fragments in  $[(\text{NH}_2)_3\text{Cr}-\text{NO}-\text{V}(\text{NH}_2)_3]$ ,  $[(\text{NH}_2)_3\text{Mo}-\text{NO}-\text{Nb}(\text{NH}_2)_3]$ ,  $[(\text{NH}_2)_3\text{Mo}-\text{NN}-\text{Mo}(\text{NH}_2)_3]$  and  $[(\text{NH}_2)_3\text{Re}-\text{CO}-\text{Ta}(\text{NH}_2)_3]$ . The numerical values given in parentheses represent the relative percentage contributions to the orbital composition from the corresponding individual atoms.

**Table 3** Relative change ( $\Delta E_{\text{O}}$ ) in the orbital interaction energy on removal of the unoccupied metal-based  $\sigma$  and small molecule  $\pi^*$  orbitals, respectively, in  $[(\text{NH}_2)_3\text{M}-\text{L}^1\text{L}^2-\text{M}'(\text{NH}_2)_3]$  systems. Results correspond to  $C_s$  symmetry

$[(\text{NH}_2)_3\text{M}-\text{L}^1\text{L}^2-\text{M}'(\text{NH}_2)_3]$	$\Delta E_{\text{O}}(\sigma)/\text{eV}$	$\Delta E_{\text{O}}(\pi)/\text{eV}$
$[(\text{NH}_2)_3\text{Cr}-\text{NO}-\text{V}(\text{NH}_2)_3]$	1.73	5.48
$[(\text{NH}_2)_3\text{Mo}-\text{NO}-\text{Nb}(\text{NH}_2)_3]$	1.89	6.05
$[(\text{NH}_2)_3\text{Mo}-\text{NN}-\text{Mo}(\text{NH}_2)_3]$	2.59	3.82
$[(\text{NH}_2)_3\text{Re}-\text{CO}-\text{Ta}(\text{NH}_2)_3]$	3.03	3.42

d orbitals as the transition metal groups are descended, allowing for greater orbital and density overlap between fragments, which is reflected in the greater values for the corresponding bonding energy components. In the case of the two 4d systems, the somewhat larger  $E_{\text{P}}$  and  $E_{\text{E}}$  values found for  $[(\text{NH}_2)_3\text{Mo}-\text{NN}-\text{Mo}(\text{NH}_2)_3]$  compared with  $[(\text{NH}_2)_3\text{Mo}-\text{NO}-\text{Nb}(\text{NH}_2)_3]$  appear to be associated with weaker Nb–O rather than Mo–N interactions.

The orbital interaction term can be partitioned into contributions from each of the  $a_1$ ,  $a_2$ , and  $e$  irreducible representations of the  $C_{3v}$  point group applicable to the dinuclear species. The  $a_1$  and  $e$  contributions arise from the  $\sigma$  and  $\pi$  interactions, respectively. The  $a_2$  contribution is omitted from Table 2 as there are no orbital interactions of this symmetry, and consequently its value is negligible. Since the  $\sigma$  and  $\pi$  interactions span different irreducible representations, it is possible to examine their effects independently. All four systems show a larger  $\pi$  than  $\sigma$  component, a result that is consistent with the greater degree of fragment orbital mixing observed in Fig. 7 for the  $\pi$  compared to  $\sigma$  interactions. The charge analysis in Table 4 also reflects the predominance of  $\pi$  over  $\sigma$  interactions, since the values on the small molecule are more negative, whilst those on the metal atoms are more positive, than the corresponding values for the separated fragments. This is in accord with the  $\pi$  back donation from the metal to small molecule fragments being more significant than the  $\sigma$  forward donation from the small molecule to metal fragments.

**Table 4** Selected structural parameters and population analysis results for  $[(\text{NH}_2)_3\text{M}-\text{L}^1\text{L}^2-\text{M}'(\text{NH}_2)_3]$  systems. Results correspond to  $C_{3v}$  symmetry

$[(\text{NH}_2)_3\text{M}-\text{L}^1\text{L}^2-\text{M}'(\text{NH}_2)_3]$	Distance/pm			Mulliken charge			
	M–L <sup>1</sup>	L <sup>1</sup> –L <sup>2</sup>	L <sup>2</sup> –M'	M	L <sup>1</sup>	L <sup>1</sup>	M'
$[(\text{NH}_2)_3\text{Cr}-\text{NO}-\text{V}(\text{NH}_2)_3]$	165.6	122.5	188.3	1.17	-0.09	-0.40	1.49
$[(\text{NH}_2)_3\text{Mo}-\text{NO}-\text{Nb}(\text{NH}_2)_3]$	178.9	124.1	198.7	1.65	-0.23	-0.48	1.80
$[(\text{NH}_2)_3\text{Mo}-\text{NN}-\text{Mo}(\text{NH}_2)_3]$	184.6	120.1	184.9	1.71	-0.40	-0.40	1.71
$[(\text{NH}_2)_3\text{Re}-\text{CO}-\text{Ta}(\text{NH}_2)_3]$	180.1	122.7	198.5	1.36	-0.01	-0.53	1.70



For all four systems, the principal contribution to the  $a_1$  component of the orbital interaction energy can be described as a donor–acceptor interaction between occupied  $\sigma$  orbitals on the small molecule fragment and unoccupied metal-based  $d_{z^2}$  orbitals. The results in Table 2 show a correlation with the trends in  $d_{\sigma}(\text{M})-\sigma(\text{L}^1\text{L}^2)$  gaps, denoted  $\Delta E(\sigma)$  in Table 1, and the increasing size of the  $d$  orbitals as the transition metal groups are descended. Larger  $E_{\text{O}}(a_1)$  values are predicted for the systems with smaller gaps and more dilated metal-based orbitals.

The  $e$  component of the orbital interaction energy is primarily associated with the interaction between the occupied metal-based  $d_{xz}$ ,  $d_{yz}$  ( $d_{\pi}$ ) orbitals and unoccupied or partially occupied  $\pi^*$  levels on the small molecule fragment. However, the overall bonding mechanism is different in the nitric oxide case from that in dinitrogen and carbon monoxide. In the latter, the  $\pi$  interaction is of the donor–acceptor type, whereas the presence of an electron in the  $\pi^*$  levels of nitric oxide implies that, for  $[(\text{NH}_2)_3\text{Cr}-\text{NO}-\text{V}(\text{NH}_2)_3]$  and  $[(\text{NH}_2)_3\text{Mo}-\text{NO}-\text{Nb}(\text{NH}_2)_3]$ , both donor–acceptor and electron pairing effects are involved.

The  $E_{\text{O}}(e)$  values in Table 2 correspond to the overall  $\pi$  interactions and, analogous to the  $E_{\text{O}}(a_1)$  component, a correlation with the trends in  $d_{\pi}(\text{M})-\pi^*(\text{L}^1\text{L}^2)$  gaps, denoted  $\Delta E(\pi)$  in Table 1, is also observed. The smallest gaps and largest  $E_{\text{O}}(e)$  values are found for the N–O systems, whilst  $[(\text{NH}_2)_3\text{Re}-\text{CO}-\text{Ta}(\text{NH}_2)_3]$  has the largest gaps and smallest  $E_{\text{O}}(e)$  values. It should be noted that in this case, only the [Re–CO] gaps are considered, as the orbital analysis (Fig. 7) indicates that the Ta contribution to the  $d_{\pi}(\text{M})-\pi^*(\text{L}^1\text{L}^2)$  interaction is much smaller. Although  $[(\text{NH}_2)_3\text{Cr}-\text{NO}-\text{V}(\text{NH}_2)_3]$  has the smallest gaps of all four systems, the more contracted 3d metal orbitals are most likely responsible for its smaller  $E_{\text{O}}(e)$  value relative to  $[(\text{NH}_2)_3\text{Mo}-\text{NO}-\text{Nb}(\text{NH}_2)_3]$ .

In the fragment analysis of  $[(\text{NH}_2)_3\text{M}-\text{L}^1\text{L}^2-\text{M}'(\text{NH}_2)_3]$  systems, the  $E_{\text{O}}(a_1)$  and  $E_{\text{O}}(e)$  contributions involve  $\sigma$  and  $\pi$  forward and back bonding interactions, respectively, and for the N–O systems there is also a combination of donor–acceptor and electron pairing effects in the  $\pi$  bonding mechanism. Thus, in order to distinguish between these interactions, it is necessary to perform additional energy decomposition analyses, where the unoccupied metal-based  $\sigma$  orbitals or the unoccupied  $\pi^*$  orbitals of the small molecule are removed. The difference in the orbital interaction energy between these and previous analyses can be used to measure the  $\sigma$  forward and  $\pi$  back bonding interactions.

The change in the  $a_1$  orbital interaction energy, denoted  $\Delta E_{\text{O}}(\sigma)$  in Table 3, provides a measure of the small molecule to metal,  $\sigma(\text{L}^1\text{L}^2)-d_{\sigma}(\text{M})$ , forward bonding interaction. Similar trends are observed across all four systems, in that the  $\Delta E_{\text{O}}(\sigma)$  values comprise 72–77% of the value of the  $E_{\text{O}}(a_1)$  term, indicating that the forward bonding process is the principal contribution to the overall  $\sigma$  interaction. In the case of the  $\pi$  interaction, the fact that nitric oxide has partially occupied  $\pi^*$  levels requires that calculations be undertaken using  $C_s$  symmetry, in order to separate the two degenerate  $\pi$  orbitals in  $C_{3v}$  symmetry into  $a'$  and  $a''$  representations. Whilst the  $a'$  component has both  $\sigma$  and  $\pi$  contributions, the  $a''$  component contains contributions of exclusively  $\pi$  character. Consequently, removal of the unoccupied  $a''$  orbital on the small molecule fragments allows for a relative measure of the metal to small molecule,  $d_{\pi}(\text{M})-\pi^*(\text{L}^1\text{L}^2)$ , back donation, corresponding to the change in the orbital interaction energy denoted  $\Delta E_{\text{O}}(\pi)$  in Table 3. The  $\Delta E_{\text{O}}(\pi)$  values in Table 3

are rather larger for the N–O compared to N–N and C–O systems and, as mentioned in the discussion of the  $E_{\text{O}}(e)$  trends, this result can be rationalized on the basis of the smaller  $d_{\pi}(\text{M})-\pi^*(\text{L}^1\text{L}^2)$  orbital gaps for  $[(\text{NH}_2)_3\text{Cr}-\text{NO}-\text{V}(\text{NH}_2)_3]$  and  $[(\text{NH}_2)_3\text{Mo}-\text{NO}-\text{Nb}(\text{NH}_2)_3]$ , which lead to stronger overlap between the relevant fragment orbitals.

It should be noted that since dinitrogen and carbon monoxide possess two unoccupied  $\pi^*$  orbitals, the  $\Delta E_{\text{O}}(\pi)$  values obtained using  $C_s$  symmetry for  $[(\text{NH}_2)_3\text{Mo}-\text{NN}-\text{M}(\text{NH}_2)_3]$  and  $[(\text{NH}_2)_3\text{Re}-\text{CO}-\text{Ta}(\text{NH}_2)_3]$  must be doubled in order to be used as a measure of the full back donation effects associated with complete removal of the unoccupied small molecule  $\pi^*$  orbitals. The resulting values are then consistent with those obtained for equivalent [W–W] and [Re–Ta] systems from previous calculations using  $C_{3v}$  symmetry.<sup>18</sup> For  $[(\text{NH}_2)_3\text{Mo}-\text{NN}-\text{M}(\text{NH}_2)_3]$  and  $[(\text{NH}_2)_3\text{Re}-\text{CO}-\text{Ta}(\text{NH}_2)_3]$ , these values represent approximately 80 and 90%, respectively, of the  $E_{\text{O}}(e)$  term, implying that the  $\pi$  back bonding interaction is the dominant contribution to the overall  $\pi$  interaction in these two systems.

For the nitric oxide case, the overall  $\pi$  interaction is a combination of donor–acceptor and electron-pairing contributions. The  $\Delta E_{\text{O}}(\pi)$  values in Table 3 are obtained from calculations where the  $a''$  ( $\pi^*$ ) orbitals are unoccupied and can thus be associated with a measure for the back bonding contribution, which possesses donor–acceptor character. These values represent approximately 54–57% of the total  $E_{\text{O}}(e)$  term, suggesting that the donor–acceptor and electron pairing mechanisms are of relatively similar importance to the overall  $\pi$  interaction in the two N–O systems.

## 4 Conclusion

The activation and scission of the N–O bond in nitric oxide using dinuclear mixed-metal species, containing transition elements with  $d^3$  and  $d^2$  configurations and trisamide ligand systems, have been investigated by means of density functional calculations. The general results from the present study confirm the findings from our previous work, based on the analysis of bond energy trends, that a  $[d^3d^2]$  metal combination is well suited for the cleavage of the N–O bond.

As previously observed for the related cases of dinitrogen and carbon monoxide, the most favourable results have been obtained with 5d systems, but cleavage is predicted for metal combinations from all transition (3d, 4d, 5d) series, including the [Cr(III)–V(III)] system, where 3d metals are exclusively involved. In contrast, the considerable stronger N–N and C–O bonds render the cleavage of dinitrogen and carbon monoxide not possible by first row transition metal systems. These computational investigations thus provide an additional example (to those experimentally reported) of the viability of using first row transition metals in processes involving N–O bond cleavage, and in this instance, with a class of metal complexes characterized by their versatility and applicability across a range of small molecule systems.

In contrast to the cleavage of dinitrogen by three-coordinate Mo complexes, where the dinuclear intermediate possesses an approximately linear [Mo–NN–Mo] core, the [M–NO–M'] core must undergo significant bending in order to stabilize the dinuclear species relative to the nitrosyl encounter complex. The experimental observation that the reaction of nitric oxide with three-coordinate  $\text{Mo}[\text{N}(\text{R})\text{Ar}]_3$  ( $\text{R} = t\text{-Bu}$ ) systems does not proceed

beyond formation of the encounter complex ( $[\text{Ar}(\text{R})\text{N}]_3\text{Mo}-\text{NO}$ ) can most likely be attributed to the steric effects of the bulky amide ligands that may prevent the  $[\text{Mo}-\text{NO}-\text{Mo}]$  core from bending enough to stabilize the dinuclear intermediate.

The comparative bonding analysis of nitric oxide, dinitrogen, and carbon monoxide activation has shown that the  $\pi$  interactions between the metal and small molecule fragments play an appreciably greater role than the corresponding  $\sigma$  interactions in the bonding across the  $[\text{M}-\text{L}^1\text{L}^2-\text{M}']$  moiety and, consequently, the activation of the  $\text{L}^1-\text{L}^2$  bond. The energy gaps between the relevant  $\pi$ -like orbitals on the metal and small molecule fragments are significantly smaller than for their  $\sigma$ -like counterparts, a fact that is reflected in greater mixing of the fragment orbitals and larger orbital interaction energy for  $\pi$  compared to  $\sigma$  bonding. For the three small molecules considered, the  $\pi$  energy gap decreases in the order  $[\text{NO} < \text{N}_2 < \text{CO}]$  and, consequently, for each individual  $\pi$  orbital interaction, the back donation between the metal and small molecule increases in the order  $[\text{CO} < \text{N}_2 < \text{NO}]$ . This dominant role of  $\pi$  bonding is consistent with previous findings that suggest that optimization of the  $\pi$  interactions (for example, ligand rotation that enhances the metal to small molecule back donation) is central to achieving increased activation.

## Acknowledgements

The authors gratefully acknowledge the Australian Research Council for financial support and the Australian National University for access to the APAC (Australian Partnership for Advanced Computing) facilities.

## References

- 1 G. B. Richter-Addo, P. Legzdins and J. Burstyn, *Chem. Rev.*, 2002, **102**, 857.
- 2 P. C. Ford and I. M. Lorkovic, *Chem. Rev.*, 2002, **102**, 993.
- 3 T. W. Hayton, P. Legzdins and W. B. Sharp, *Chem. Rev.*, 2002, **102**, 935.
- 4 A. L. Odom and C. C. Cummins, *J. Am. Chem. Soc.*, 1995, **117**, 6613.
- 5 A. S. Veige, L. M. Slaughter, E. B. Lobkovsky, P. T. Wolczanski, N. Matsunaga, S. A. Decker and T. R. Cundari, *Inorg. Chem.*, 2003, **42**, 6204.
- 6 C. E. Laplaza and C. C. Cummins, *Science*, 1995, **268**, 861.
- 7 C. E. Laplaza, M. J. A. Johnson, J. C. Peters, A. L. Odom, E. Kim, C. C. Cummins, G. N. George and I. J. Pickering, *J. Am. Chem. Soc.*, 1996, **118**, 8623.
- 8 C. C. Cummins, *Chem. Commun.*, 1998, 1777.
- 9 J. R. Postgate, *Nitrogen Fixation*, Cambridge University Press, Cambridge, 1998.
- 10 J.-P. F. Cherry, A. R. Johnson, L. M. Baraldo, Y.-C. Tsai, C. C. Cummins, S. V. Kryatov, E. V. Rybak-Akimova, K. B. Capps, C. D. Hoff, C. M. Haar and S. P. Nolan, *J. Am. Chem. Soc.*, 2001, **123**, 7271.
- 11 C. E. Laplaza, A. L. Odom, W. M. Davis, C. C. Cummins and J. D. Protasiewicz, *J. Am. Chem. Soc.*, 1995, **117**, 4499.
- 12 J. C. Peters, A. L. Odom and C. C. Cummins, *Chem. Commun.*, 1997, 1995.
- 13 J. B. Greco, J. C. Peters, T. A. Baker, W. M. Davis, C. C. Cummins and G. Wu, *J. Am. Chem. Soc.*, 2001, **123**, 5003.
- 14 J. C. Peters, L. M. Baraldo, T. A. Baker, A. R. Johnson and C. C. Cummins, *J. Organomet. Chem.*, 1999, **591**, 24.
- 15 G. J. Christian, R. Stranger and B. F. Yates, *Inorg. Chem.*, 2006, **45**, 6851.
- 16 A. Ariafard, N. Brookes, R. Stranger and B. F. Yates, *J. Am. Chem. Soc.*, 2008, **130**, 11928.
- 17 G. Christian, R. Stranger, S. Petrie, B. F. Yates and C. C. Cummins, *Chem.-Eur. J.*, 2007, **13**, 4264.
- 18 G. Christian, R. Stranger, B. F. Yates and C. C. Cummins, *Dalton Trans.*, 2008, 338.
- 19 E. J. Baerends, J. Autschbach, A. Bérce, F. M. Bickelhaupt, C. Bo, P. M. Boerrigter, L. Cavallo, D. P. Chong, L. Deng, R. M. Dickson, D. E. Ellis, M. van Faassen, L. Fan, T. H. Fischer, C. Fonseca Guerra, S. J. A. van Gisbergen, A. W. Götz, J. A. Groeneveld, O. V. Gritsenko, M. Grüning, F. E. Harris, P. van den Hoek, C. R. Jacob, H. Jacobsen, L. Jensen, G. van Kessel, F. Kootstra, M. V. Krykunov, E. van Lenthe, D. A. McCormack, A. Michalak, J. Neugebauer, V. P. Nicu, V. P. Osinga, S. Patchkovskii, P. H. T. Philipsen, D. Post, C. C. Pye, W. Ravenek, J. I. Rodriguez, P. Ros, P. R. T. Schipper, G. Schreckenbach, J. G. Snijders, M. Solà, M. Swart, D. Swerhone, G. te Velde, P. Vernooijs, L. Versluis, L. Visscher, O. Visser, F. Wang, T. A. Wesolowski, E. M. van Wezenbeek, G. Wiesenekker, S. K. Wolff, T. K. Woo, A. L. Yakovlev, T. Ziegler, *ADF, SCM, Theoretical Chemistry*, Vrije Universiteit, Amsterdam, The Netherlands, <http://www.scm.com>.
- 20 C. Fonseca Guerra, J. G. Snijders, G. te Velde and E. J. Baerends, *Theor. Chem. Acc.*, 1998, **99**, 391.
- 21 G. te Velde, F. M. Bickelhaupt, S. J. A. van Gisbergen, C. Fonseca Guerra, E. J. Baerends, J. G. Snijders and T. Ziegler, *J. Comput. Chem.*, 2001, **22**, 931.
- 22 A. D. Becke, *Phys. Rev. A: At., Mol., Opt. Phys.*, 1988, **38**, 3098.
- 23 J. P. Perdew, *Phys. Rev. B: Condens. Matter Mater. Phys.*, 1986, **33**, 8822.
- 24 E. van Lenthe, E. J. Baerends and J. G. Snijders, *J. Chem. Phys.*, 1993, **99**, 4597.
- 25 E. van Lenthe, E. J. Baerends and J. G. Snijders, *J. Chem. Phys.*, 1994, **101**, 9783.
- 26 E. van Lenthe, A. E. Ehlers and E. J. Baerends, *J. Chem. Phys.*, 1999, **110**, 8943.
- 27 A. Bérce, R. M. Dickson, L. Fan, H. Jacobsen, D. Swerhone and T. Ziegler, *Comput. Phys. Commun.*, 1997, **100**, 247.
- 28 H. Jacobsen, A. Bérce, D. P. Swerhone and T. Ziegler, *Comput. Phys. Commun.*, 1997, **100**, 263.
- 29 S. K. Wolff, *Int. J. Quantum Chem.*, 2005, **104**, 645.
- 30 MOLEKEL: An Interactive Molecular Graphics Tool, <http://www.cscs.ch/molekel/>.
- 31 S. Portmann and H. P. Lüthi, *Chimia*, 2000, **54**, 766.
- 32 MOLDEN: A Pre and Post Processing Program for Molecular and Electronic Structures, <http://www.cmbi.ru.nl/molden/molden.html>.
- 33 G. Schaftenaar and J. H. Noordik, *J. Comput.-Aided Mol. Des.*, 2000, **14**, 123.
- 34 G. Christian, J. Driver and R. Stranger, *Faraday Discuss.*, 2003, **124**, 331.
- 35 G. Christian and R. Stranger, *Dalton Trans.*, 2004, 2492.
- 36 G. Christian, R. Stranger, B. F. Yates and D. C. Graham, *Dalton Trans.*, 2005, 962.
- 37 G. Christian, R. Stranger, B. F. Yates and C. C. Cummins, *Dalton Trans.*, 2007, 1939.
- 38 G. Christian, R. Stranger, B. F. Yates and C. C. Cummins, *Eur. J. Inorg. Chem.*, 2007, 3736.
- 39 M. Güell, J. M. Luis, M. Solà and M. Swart, *J. Phys. Chem. A*, 2008, **112**, 6384.
- 40 T. Ziegler and A. Rauk, *Inorg. Chem.*, 1979, **18**, 1558.
- 41 T. Ziegler and A. Rauk, *Inorg. Chem.*, 1979, **18**, 1755.
- 42 F. M. Bickelhaupt and E. J. Baerends, *Rev. Comput. Chem.*, 2000, **15**, 1.